Spectral collocation method for collisional power absorption in radially inhomogeneous helicon plasmas

Suwon Cho*
Department of Physics, Kyonggi University, Suwon, Kyonggi-Do 16227, Republic of Korea

(Received 8 November 2018; published 18 March 2019)

A spectral collocation method using Chebyshev polynomials is applied to compute the electromagnetic fields and the collisional power absorption in radially inhomogeneous helicon plasmas. The governing equation has a singularity at the cylindrical axis, which has been resolved by imposing the appropriate boundary conditions. The results are compared with those of the finite difference method. The present work not only shows the superior accuracy of the spectral collocation method with a proper treatment of the singularity, but also discusses the advantages of using Chebyshev nodes for helicon plasmas in particular. It is possible to extend the range of parameters efficiently in cases for which the finite difference method fails to obtain reliable solutions without drastically decreasing the grid size. The spectral collocation method is shown to be especially useful near the lower hybrid resonance condition.

DOI: 10.1103/PhysRevE.99.033303

I. INTRODUCTION

Helicon discharge has been of great interest mainly in view of its high ionization efficiency and its applications in many areas such as basic plasma and fusion experiments, material processing reactors, and plasma thrusters. Typical characteristics of helicon plasmas include the linear dependence of the density on the magnetic field [1], occurrence of abrupt density jumps [1–3], and the existence of density peaks at low magnetic fields [4–7] and near the lower hybrid resonance [1,8–12]. These characteristics can be explained with power balance in which the absorbed power equals the power lost in the plasma [13–15]. The power absorption has been investigated by many researchers [16–26], and its computation has recently been performed to analyze characteristics of discharges [27–29].

The high efficiency of ionization appears to be attributed to collisional damping of the Trivelpiece-Gould (TG) mode, at least in part, which exists with the helicon wave [18,25,30–34]. Mainly because of the short wavelength of the TG mode, computing the wave electromagnetic fields and the power absorption accurately is not trivial, depending on the values of various parameters. In fact, the operating ranges of wave and plasma parameters are quite wide. For example, the density is up to the order of 10^{14} cm^{-3}, the magnetic field up to a few kG, and the frequency range up to 10^2 MHz.

For radially inhomogeneous plasmas, the Maxwell equations reduce to a system of ordinary differential equations that can be solved by using various numerical methods, such as the finite difference [7,35–38], finite element [30], direct integration [20,24,31,39], and stratified model methods [19,40]. In the stratified model, the continuous profile of the plasma parameters is replaced with a stepwise variation, then the analytic solutions in each stratum are matched at the interfaces to obtain the solution in the entire region.

By treating the problem as an initial value problem, it is relatively simple and straightforward to apply the integration method using many standard libraries, but it may yield unreliable results in certain but quite wide ranges of the wave and plasma parameters because the governing differential equations can be stiff. In such a case, a method using a series expansion in the electron mass might be used to obtain the approximate solutions [24].

The finite difference method [7,35–38] and the finite element method [30] have also been applied for numerical modeling of helicon plasmas. These methods are less sensitive to the parameter range, but the accuracy may not be assured in some cases. The accuracy might be improved by decreasing the mesh size, but its convergence rate with varying mesh size is generally slow [41–43]. Compared to these methods using expansion of local interpolant polynomials, the accuracy of the spectral collocation method is known to be excellent with a minimal number of computational nodes. In the spectral method, the solutions is expanded as a global interpolant, and the Chebyshev polynomials are the natural choice for bounded, nonperiodic domains among various polynomials [41,42]. In addition, it is especially advantageous to adapt the Chebyshev polynomials for helicon plasmas because they are based on the node points highly clustered near the boundary, where the TG mode can vary rapidly with significant damping.

In this work, a spectral collocation method using the Chebyshev differentiation matrix is applied to the helicon plasma configuration, and its superior accuracy and advantages are demonstrated by comparing the results with those of the finite difference method. The spectral collocation method is sometimes called just the spectral method for the sake of brevity in this paper.

II. MODEL

As in previous works [7,39], it is assumed that the plasma is confined in the region $0 \leqslant r \leqslant r_p$ and that there are an antenna

*swcho@kgu.ac.kr

and a conducting wall at r_a and r_b, respectively. The electromagnetic fields are governed by the Maxwell equations, which may be written as

$$\hat{\nabla} \times \mathbf{E} = -\boldsymbol{\mathcal{H}}, \tag{1}$$

$$\hat{\nabla} \times \boldsymbol{\mathcal{H}} = \boldsymbol{\epsilon} \cdot \mathbf{E}, \tag{2}$$

where $\hat{\nabla} = (c/\omega)\nabla$, $\boldsymbol{\mathcal{H}} = i\sqrt{\mu_0/\epsilon_0}\mathbf{H}$, and $\boldsymbol{\epsilon}$ is the dielectric tensor of a cold plasma in the form

$$\boldsymbol{\epsilon} = \begin{bmatrix} \epsilon_1 & i\epsilon_2 & 0 \\ -i\epsilon_2 & \epsilon_1 & 0 \\ 0 & 0 & \epsilon_3 \end{bmatrix}. \tag{3}$$

Here c, ϵ_0, and μ_0 are the speed of light, the permittivity, and the permeability of free space, respectively. It is assumed that the plasma is uniform in the azimuthal and axial directions and that the first-order electromagnetic fields vary as $\exp[i(m\theta + kz - \omega t)]$. Then the Maxwell equations reduce to a set of ordinary differential equations with respect to the radial coordinate:

$$\frac{d\mathbf{u}}{d\rho} + \mathbf{L} \cdot \mathbf{u} = 0, \tag{4}$$

$$\mathbf{L} = \begin{pmatrix} \frac{1}{\rho} - \frac{m\epsilon_2}{\rho\epsilon_1} & 0 & -\frac{mN_\parallel}{\rho\epsilon_1} & \frac{m^2}{\rho^2\epsilon_1} - 1 \\ -N_\parallel\frac{\epsilon_2}{\epsilon_1} & 0 & 1 - \frac{N_\parallel^2}{\epsilon_1} & \frac{mN_\parallel}{\rho\epsilon_1} \\ -\frac{mN_\parallel}{\rho} & \frac{m^2}{\rho^2} - \epsilon_3 & \frac{1}{\rho} & 0 \\ \epsilon_1 - \frac{\epsilon_2^2}{\epsilon_1} - N_\parallel^2 & \frac{mN_\parallel}{\rho} & -N_\parallel\frac{\epsilon_2}{\epsilon_1} & \frac{m\epsilon_2}{\rho\epsilon_1} \end{pmatrix}, \tag{5}$$

where $\mathbf{u} = (E_\theta, E_z, \mathcal{H}_\theta, \mathcal{H}_z)^{\mathrm{T}}$, $N_\parallel = kc/\omega$, and $\rho = r\omega/c$. The superscript T denotes the transpose. The radial field components are given in terms of the other components as

$$\mathcal{H}_r = \frac{m}{\rho}E_z - N_\parallel E_\theta, \tag{6}$$

$$\epsilon_1 E_r = \frac{m}{\rho}\mathcal{H}_z - N_\parallel \mathcal{H}_\theta - \epsilon_2 E_\theta. \tag{7}$$

When the plasma is uniform in the radial direction too, the fields are given in terms of Bessel functions, whose argument is $N_\perp \rho$ where $N_\perp$ is the root of the biquadratic equation [18]

$$N_\perp^4 - (\alpha + \beta)N_\perp^2 + \alpha\beta - \gamma\delta = 0, \tag{8}$$

with $\alpha = \epsilon_3(1 - N_\parallel^2/\epsilon_1)$, $\beta = \epsilon_1 - N_\parallel^2 - \epsilon_2^2/\epsilon_1$, $\gamma = N_\parallel\epsilon_2/\epsilon_1$, and $\delta = N_\parallel\epsilon_2\epsilon_3/\epsilon_1$. There are two solutions for $N_\perp^2$, related to the fast and slow waves, that are usually called the helicon and TG modes in helicon plasmas.

The power absorbed by the plasma can be expressed as $P_{\mathrm{abs}} = 1/2R_{\mathrm{p}}I_a^2$ where I_a is the antenna current and R_{p} is the plasma resistance given by

$$R_{\mathrm{p}} = \sum_m \int_{-\infty}^{\infty} S_{\mathrm{p}}(m,k)\,dk, \tag{9}$$

$$S_{\mathrm{p}}(m,k) = \frac{4\pi^2\epsilon_0\omega}{I_a^2}\int_0^{r_p} \mathrm{Im}[\mathbf{E}^* \cdot \boldsymbol{\epsilon} \cdot \mathbf{E}] r\,dr, \tag{10}$$

where r_p is the plasma boundary radius. The absorbed power must be equal to the power radiated by the antenna calculated from

$$S_{\mathrm{a}}(m,k) = \frac{4\pi^2}{I_a^2}\int_0^{r_p} \mathrm{Re}[\mathbf{J}_a \cdot \mathbf{E}^*] r\,dr, \tag{11}$$

where $\mathbf{J}_a$ is the antenna current density.

III. SPECTRAL COLLOCATION METHOD

A. Series expansion

A function $f(\xi)$ can be approximated by the series,

$$f(\xi) \simeq \sum_{j=1}^{n} f_j \phi_j(\xi), \tag{12}$$

where $\{\xi_j\}$ and $\{\phi_j\}$ are sets of distinct interpolation nodes and interpolating functions, respectively, $f_j = f(\xi_j)$, and n is the number of nodes. By using the differentiation matrix $\{D_{i,j}\}$, the derivative at the node ξ_i is given as [42,43]

$$f'(\xi_i) \simeq \sum_{j=1}^{n} f_j \phi_j'(\xi_i) \equiv \sum_{j=1}^{n} D_{i,j} f_j. \tag{13}$$

As mentioned earlier, we use the differentiation matrix based on the Chebyshev polynomials and points. To describe the plasma confined in the range $0 \leqslant \rho \leqslant \rho_p (= r_p\omega/c)$, we may use the change of variable $\rho = \rho_p(1 - \xi)/2$ with the differentiation matrix multiplied by $-\rho_p/2$. This transform yields to highly clustered points near both the origin and the boundary at ρ_p. The existence of clustered points in the small region near the origin is not efficient unless the function has a strong gradient and narrow peaks there [42,44].

The quadratic transform

$$\rho^2 = \tfrac{1}{2}\rho_p^2(1 - \xi) \tag{14}$$

leads to clustering of grid points only near ρ_p and generally better accuracy [44]. In addition, it is especially useful to have a high density of grid points near the boundary ρ_p, where the TG mode can vary rapidly.

B. Boundary conditions

Equation (5) has a singularity at the origin, which should be resolved to obtain proper solutions in the entire domain. Using the boundary conditions instead of Eqs. (4) and (5), we can set up the relation between $d\mathbf{u}/d\rho$ (and then $d\mathbf{u}/d\xi$) and $\mathbf{u}$ at the origin. Noting that the field components should be independent of θ as $\rho \to 0$ [45], we obtain the boundary conditions at $\rho = 0$ as

$$E_r = E_\theta = 0, \quad \text{for} \quad m = 0, \tag{15}$$

$$E_r + imE_\theta = E_z = 0, \quad \text{for} \quad |m| = 1, \tag{16}$$

$$E_r = E_\theta = E_z = 0, \quad \text{for} \quad |m| > 1. \tag{17}$$

These relations also hold for $\boldsymbol{\mathcal{H}}$.

For $m = 0$, Eqs. (4) and (5) with $E_\theta = \mathcal{H}_\theta = 0$ lead to

$$\frac{dE_z}{d\rho} = 0, \quad \frac{d\mathcal{H}_z}{d\rho} = 0, \tag{18}$$

which enable one to approximate E_θ, E_z, $\mathcal{H}_\theta$, and $\mathcal{H}_z$, with their respective leading terms in the power series as $\rho \to 0$, such as

$$E_\theta = E_1\rho, \quad \mathcal{H}_\theta = H_1\rho, \quad E_z = E_0, \quad \mathcal{H}_z = H_0, \tag{19}$$

where E_0, E_1, H_0, and H_1 are constants. The equations for $E_1 = dE_\theta/d\rho|_{\rho=0}$ and $H_1 = d\mathcal{H}_\theta/d\rho|_{\rho=0}$ in Eqs. (4) and (5) yield

$$E_1 = \tfrac{1}{2}H_0, \quad H_1 = \tfrac{1}{2}\epsilon_3 E_0. \tag{20}$$

To use $D_{i,j} = \phi_j'(\xi_i)$, we need $dE_\theta/d\xi$ and $d\mathcal{H}_\theta/d\xi$ for ξ given by Eq. (14), but as

$$\frac{dE_\theta}{d\rho} = -\frac{4\rho}{\rho_p^2}\frac{dE_\theta}{d\xi} \tag{21}$$

indicates, $dE_\theta/d\xi$ should be infinite for $dE_\theta/d\rho$ to be finite at $\rho = 0$. This problem can be circumvented by taking $u^{(1)} = \rho E_\theta$ and $u^{(3)} = \rho\mathcal{H}_\theta$ to obtain

$$\frac{dE_\theta}{d\rho} = -\frac{2}{\rho_p^2}\frac{du^{(1)}}{d\xi} \tag{22}$$

at $\rho = 0$ and to solve for $u^{(1)}$ and $u^{(3)}$ first. These substitutions will be also explained at the end of this subsection. Then Eq. (20) yields

$$\frac{du^{(1)}}{d\xi} + aH_0 = 0, \tag{23}$$

$$\frac{du^{(3)}}{d\xi} + a\epsilon_3 E_0 = 0 \tag{24}$$

or

$$au_1^{(4)} + \sum_{j=2}^{n} D_{1,j}u_j^{(1)} = 0, \tag{25}$$

$$a\epsilon_3 u_1^{(2)} + \sum_{j=2}^{n} D_{1,j}u_j^{(3)} = 0, \tag{26}$$

at $\rho = 0$, where $a = \rho_p^2/4 = \rho_n^2/4$. Here we use the notation

$$\mathbf{u}_i = \left[u_i^{(1)}, u_i^{(2)}, u_i^{(3)}, u_i^{(4)}\right]^{\mathrm{T}}, \tag{27}$$

$$= [\rho_i E_\theta(\xi_i), E_z(\xi_i), \rho_i\mathcal{H}_\theta(\xi_i), \mathcal{H}_z(\xi_i)]^{\mathrm{T}}. \tag{28}$$

For $|m| = 1$, applying Eq. (16) to Eqs. (4) and (5), we find

$$\frac{dE_\theta}{d\rho} = 0, \quad \frac{d\mathcal{H}_\theta}{d\rho} = 0. \tag{29}$$

Then E_θ, E_z, $\mathcal{H}_\theta$, and $\mathcal{H}_z$ can be also approximated with

$$E_\theta = E_0, \quad \mathcal{H}_\theta = H_0, \quad E_z = E_1\rho, \quad \mathcal{H}_z = H_1\rho, \tag{30}$$

as $\rho \to 0$, where E_0, E_1, H_0, and H_1 are constants different from the previous ones for $m = 0$. In the same way as for $m = 0$, we finally obtain

$$(m\epsilon_1 - \epsilon_2)E_0 - N_\parallel H_0 + mH_1 = 0, \tag{31}$$

$$N_\parallel E_0 - mH_0 - mE_1 = 0 \tag{32}$$

or

$$\frac{2aN_\parallel}{m}u_1^{(1)} - 2au_1^{(3)} + \sum_{j=2}^{n} D_{1,j}u_j^{(2)} = 0, \tag{33}$$

$$-2a\left(1 - \frac{\epsilon_2}{m}\right)u_1^{(1)} + \frac{2aN_\parallel}{m}u_1^{(3)} + \sum_{j=2}^{n} D_{1,j}u_j^{(4)} = 0, \tag{34}$$

where $\mathbf{u}_i = [E_\theta(\xi_i), \rho_i E_z(\xi_i), \mathcal{H}_\theta(\xi_i), \rho_i\mathcal{H}_z(\xi_i)]^{\mathrm{T}}$.

At the plasma boundary, we have the relations

$$\mathcal{H}_\theta = b_{1,1}E_\theta + b_{1,2}E_z + d_1, \tag{35}$$

$$\mathcal{H}_z = b_{2,1}E_\theta + b_{2,2}E_z + d_2, \tag{36}$$

where $\{b_{i,j}\}$ and $\{d_i\}$ are given in terms of the modified Bessel functions and the antenna current [18]. These equations should be modified as

$$u_n^{(3)} = \tilde{b}_{1,1}u_n^{(1)} + \tilde{b}_{1,2}u_n^{(2)} + \tilde{d}_1, \tag{37}$$

$$u_n^{(4)} = \tilde{b}_{2,1}u_n^{(1)} + \tilde{b}_{2,2}u_n^{(2)} + \tilde{d}_2, \tag{38}$$

where

$$\tilde{b}_{1,1} = b_{1,1}, \quad \tilde{b}_{1,2} = b_{1,2}\rho_n, \quad \tilde{d}_1 = d_1\rho_n, \tag{39}$$

$$\tilde{b}_{2,1} = \frac{b_{2,1}}{\rho_n}, \quad \tilde{b}_{2,2} = b_{2,2}, \quad \tilde{d}_2 = d_2, \tag{40}$$

for $m = 0$, and

$$\tilde{b}_{1,1} = b_{1,1}, \quad \tilde{b}_{1,2} = \frac{b_{1,2}}{\rho_n}, \quad \tilde{d}_1 = d_1, \tag{41}$$

$$\tilde{b}_{2,1} = b_{2,1}\rho_n, \quad \tilde{b}_{2,2} = b_{2,2}, \quad \tilde{d}_2 = d_2\rho_n \tag{42}$$

for $m = \pm 1$.

Because $T_{2j}(\rho) = (-1)^j T_j(1 - 2\rho^2)$ (where T_j is a Chebysheb polynomial of degree j), the change of variables by Eq. (14) is equivalent to using polynomials of even degree only. By noting that the radial and azimuthal components vary as $\rho^{|m|-1}$ or ρ for $m \geqslant 1$ or $m = 0$, respectively, and that the axial component varies as $\rho^{|m|}$ as $\rho \to 0$ [30], it is necessary to take $E_z = u^{(2)}/\rho$ and $\mathcal{H}_z = u^{(4)}/\rho$ for odd m and $E_\theta = u^{(1)}/\rho$ and $\mathcal{H}_\theta = u^{(2)}/\rho$ for even m. In other words, the same procedure for $m = 0$ or $|m| = 1$ is applied to the case of even or odd m, respectively, when $|m| > 1$. The asymptotic behavior can also be seen from the analytic solutions for a uniform plasma [18].

C. Governing equations

Using Eq. (14), we transform Eq. (4) to

$$\frac{d\mathbf{u}}{d\xi} + \mathbf{Q}\cdot\mathbf{u} = 0, \tag{43}$$

for $-1 \leqslant \xi < 1$, where the matrix $\mathbf{Q}$ can be obtained in a straightforward way for

$$\mathbf{u} = [\rho(\xi)E_\theta(\xi), E_z(\xi), \rho(\xi)\mathcal{H}_\theta(\xi), \mathcal{H}_z(\xi)]^{\mathrm{T}}, \tag{44}$$

$$\mathbf{u} = [E_\theta(\xi), \rho(\xi)E_z(\xi), \mathcal{H}_\theta(\xi), \rho(\xi)\mathcal{H}_z(\xi)]^{\mathrm{T}}, \tag{45}$$

when m is even or odd, respectively. At $\xi = 1$, the relevant equations are given by Eqs. (25) and (26) or Eqs. (33) and (34) according to whether m is even or odd, respectively.

D. Algebraic equations

Equation (13) is extended to apply for a system of equations, and then Eq. (43) is converted to an algebraic equation

$$(\mathbf{A} + \mathbf{B}) \cdot \mathbf{U} = \mathbf{R}, \tag{46}$$

$$\mathbf{A} = \begin{bmatrix} \cdot & \mathbf{A}_{1,2} & \cdots & \mathbf{A}_{1,n-1} & \mathbf{A}_{1,n} \\ \mathbf{A}_{2,1} & \mathbf{D}_{2,2} & \cdots & \mathbf{D}_{2,n-1} & \mathbf{A}_{2,n} \\ \cdot & \cdot & \cdots & \cdot & \cdot \\ \mathbf{A}_{n-1,1} & \mathbf{D}_{n-1,2} & \cdots & \mathbf{D}_{n-1,n-1} & \mathbf{A}_{n-1,n} \\ \mathbf{A}_{n,1} & \mathbf{A}_{n,2} & \cdots & \mathbf{A}_{n,n-1} & \mathbf{A}_{n,n} \end{bmatrix}, \tag{47}$$

$$\mathbf{B} = \begin{bmatrix} \mathbf{B}_{1,1} & \cdot & \cdots & \cdot & \cdot \\ \cdot & \mathbf{Q}(\xi_2) & \cdots & \cdot & \cdot \\ \cdot & \cdot & \cdots & \cdot & \cdot \\ \cdot & \cdot & \cdots & \mathbf{Q}(\xi_{n-1}) & \cdot \\ \cdot & \cdot & \cdots & \cdot & \mathbf{B}_{n,n} \end{bmatrix}, \tag{48}$$

where $\mathbf{D}_{i,j} = D_{i,j}\mathbf{I}_4$ ($\mathbf{I}_n$ is the identity matrix of size n). The single dot is used to denote a zero or a zero matrix inside a vector or matrix throughout the paper. Equation (46) is solved by a direct solver using LU decomposition.

1. Matrices for $m = 0$

When $m = 0$, the matrices $\mathbf{A}_{i,j}$ and $\mathbf{B}_{i,j}(i = 2, \ldots, n-1$ and $j = 2, \ldots, n-1)$ and the vectors $\mathbf{U}$ and $\mathbf{R}$ are given as follows:

$$\mathbf{A}_{1,j} = \begin{bmatrix} D_{1,j} & \cdot & \cdot & \cdot \\ \cdot & \cdot & D_{1,j} & \cdot \end{bmatrix}, \tag{49}$$

$$\mathbf{A}_{1,n} = \begin{bmatrix} D_{1,n} & \cdot \\ D_{1,n}\tilde{b}_{1,1} & D_{1,n}\tilde{b}_{1,2} \end{bmatrix}, \tag{50}$$

$$\mathbf{A}_{i,1} = \begin{bmatrix} \cdot & \cdot \\ D_{i,1} & \cdot \\ \cdot & \cdot \\ \cdot & D_{i,1} \end{bmatrix}, \tag{51}$$

$$\mathbf{A}_{i,n} = \begin{bmatrix} D_{i,n} & \cdot \\ \cdot & D_{i,n} \\ D_{i,n}\tilde{b}_{1,1} & D_{i,n}\tilde{b}_{1,2} \\ D_{i,n}\tilde{b}_{2,1} & D_{i,n}\tilde{b}_{2,2} \end{bmatrix}, \tag{52}$$

$$\mathbf{A}_{n,j} = \begin{bmatrix} D_{n,j} & \cdot & \cdot & \cdot \\ \cdot & D_{n,j} & \cdot & \cdot \end{bmatrix}, \tag{53}$$

$$\mathbf{A}_{n,1} = \begin{bmatrix} \cdot & \cdot \\ D_{n,1} & \cdot \end{bmatrix}, \tag{54}$$

$$\mathbf{A}_{n,n} = \begin{bmatrix} D_{n,n} & \cdot \\ \cdot & D_{n,n} \end{bmatrix}, \tag{55}$$

$$\mathbf{B}_{1,1} = \begin{bmatrix} \cdot & -a \\ -a\epsilon_3 & \cdot \end{bmatrix}, \tag{56}$$

$$\mathbf{B}_{n,n} = \begin{bmatrix} Q^{(n)}_{1,1} & Q^{(n)}_{1,2} \\ Q^{(n)}_{2,1} & Q^{(n)}_{2,2} \end{bmatrix} + \begin{bmatrix} Q^{(n)}_{1,3} & Q^{(n)}_{1,4} \\ Q^{(n)}_{2,3} & Q^{(n)}_{2,4} \end{bmatrix} \cdot \begin{bmatrix} \tilde{b}_{1,1} & \tilde{b}_{1,2} \\ \tilde{b}_{2,1} & \tilde{b}_{2,2} \end{bmatrix}, \tag{57}$$

$$\mathbf{U} = [\mathbf{u}_1, \mathbf{u}_2, \cdots, \mathbf{u}_n]^{\mathrm{T}}, \tag{58}$$

$$\mathbf{u}_1 = \left[u^{(2)}_1, u^{(4)}_1\right], \tag{59}$$

$$\mathbf{u}_i = \left[u^{(1)}_i, u^{(2)}_i, u^{(3)}_i, u^{(4)}_i\right], \tag{60}$$

$$\mathbf{u}_n = \left[u^{(1)}_n, u^{(2)}_n\right], \tag{61}$$

$$\mathbf{R} = -[\mathbf{r}_1, \mathbf{r}_2, \cdots, \mathbf{r}_{n-1}, \mathbf{r}_n]^{\mathrm{T}}, \tag{62}$$

$$\mathbf{r}_1 = [\cdot\ , D_{1,n}\tilde{d}_1]^{\mathrm{T}}, \tag{63}$$

$$\mathbf{r}_i = [\cdot\ , \cdot\ , D_{i,n}\tilde{d}_1, D_{i,n}\tilde{d}_2]^{\mathrm{T}}, \tag{64}$$

$$\mathbf{r}_n = \left[Q^{(n)}_{1,3}\tilde{d}_1 + Q^{(n)}_{1,4}\tilde{d}_2, Q^{(n)}_{2,3}\tilde{d}_1 + Q^{(n)}_{2,4}\tilde{d}_2\right]^{\mathrm{T}}, \tag{65}$$

where $Q^{(n)}_{i,j} = Q_{i,j}(\xi_n)$.

2. Matrices for $|m| = 1$

The boundary conditions at the origin for $m = \pm 1$ give rise to slightly different entries in the first two rows and columns of the matrices and the first two rows of the vectors obtained previously. The matrices and vectors that are different from those for $m = 0$ are listed as follows:

$$\mathbf{A}_{1,j} = \begin{bmatrix} \cdot & D_{1,j} & \cdot & \cdot \\ \cdot & \cdot & \cdot & D_{1,j} \end{bmatrix}, \tag{66}$$

$$\mathbf{A}_{1,n} = \begin{bmatrix} \cdot & D_{1,n} \\ D_{1,n}\tilde{b}_{2,1} & D_{1,n}\tilde{b}_{2,2} \end{bmatrix}, \tag{67}$$

$$\mathbf{A}_{i,1} = \begin{bmatrix} D_{i,1} & \cdot \\ \cdot & \cdot \\ \cdot & D_{i,1} \\ \cdot & \cdot \end{bmatrix}, \tag{68}$$

$$\mathbf{A}_{n,1} = \begin{bmatrix} D_{n,1} & \cdot \\ \cdot & \cdot \end{bmatrix}, \tag{69}$$

$$\mathbf{B}_{1,1} = 2a \begin{bmatrix} -\frac{N_\parallel}{m} & 1 \\ \epsilon_1 - \frac{\epsilon_2}{m} & -\frac{N_\parallel}{m} \end{bmatrix}, \tag{70}$$

$$\mathbf{u}_1 = \left[u^{(1)}_1, u^{(3)}_1\right], \tag{71}$$

$$\mathbf{r}_1 = [\cdot\ , D_{1,n}\tilde{d}_2]^{\mathrm{T}}. \tag{72}$$

3. Matrices for $|m| > 1$

Because $E_\theta = E_z = \mathcal{H}_\theta = \mathcal{H}_z = 0$ for $|m| > 1$, the system of equations is simply obtained by deleting the first two rows and two columns of the matrices $\mathbf{A}$ and $\mathbf{B}$ and the first two rows of the vectors $\mathbf{U}$ and $\mathbf{R}$.

IV. FINITE DIFFERENCE METHOD

For comparison of methods, the finite difference method is reviewed in this section. Using the approximations with second-order error in $h_{i+\frac{1}{2}}$,

$$\left.\frac{du}{d\rho}\right|_{\rho_{i+\frac{1}{2}}} \simeq \frac{-u_i + u_{i+1}}{h_{i+\frac{1}{2}}}, \tag{73}$$

$$u(\rho_{i+\frac{1}{2}}) \simeq \tfrac{1}{2}(u_i + u_{i+1}), \tag{74}$$

where $h_{i+\frac{1}{2}} = \rho_{i+1} - \rho_i$, $\rho_{i+\frac{1}{2}} = (\rho_i + \rho_{i+1})/2$, and i is the node number, Eq. (4) is discretized as

$$(\mathbf{A} + \mathbf{B}) \cdot \mathbf{U} = \mathbf{R}, \tag{75}$$

where

$$\mathbf{A} = \begin{bmatrix} \mathbf{A}^{(1)} & \mathbf{D}_+ & \cdot & \cdots & \cdot & \cdot \\ \cdot & \mathbf{D}_- & \mathbf{D}_+ & \cdots & \cdot & \cdot \\ \cdot & \cdot & \cdot & \cdots & \cdot & \cdot \\ \cdot & \cdot & \cdot & \cdots & \mathbf{D}_+ & \cdot \\ \cdot & \cdot & \cdot & \cdots & \mathbf{D}_- & \mathbf{A}^{(n-1)} \end{bmatrix}, \tag{76}$$

$$\mathbf{B} = \begin{bmatrix} \mathbf{B}_-^{(1)} & \mathbf{B}^{(1)} & \cdot & \cdots & \cdot & \cdot \\ \cdot & \mathbf{B}^{(2)} & \mathbf{B}^{(2)} & \cdots & \cdot & \cdot \\ \cdot & \cdot & \cdot & \cdots & \cdot & \cdot \\ \cdot & \cdot & \cdot & \cdots & \mathbf{B}^{(n-2)} & \cdot \\ \cdot & \cdot & \cdot & \cdots & \mathbf{B}^{(n-1)} & \mathbf{B}_+^{(n-1)} \end{bmatrix}, \tag{77}$$

$$\mathbf{D}_\pm = \pm\mathbf{I}_4, \quad \mathbf{B}^{(i)} = \tfrac{1}{2}h_{i+\frac{1}{2}}\mathbf{L}(\rho_{i+\frac{1}{2}}), \tag{78}$$

$$\mathbf{U} = [\mathbf{u}_1, \mathbf{u}_2, \cdots, \mathbf{u}_n]^{\mathrm{T}}, \tag{79}$$

$$\mathbf{u}_i = [E_\theta(\rho_i), E_z(\rho_i), \mathcal{H}_\theta(\rho_i), \mathcal{H}_z(\rho_i)]^{\mathrm{T}}, \tag{80}$$

$$\mathbf{u}_n = [E_\theta(\rho_n), E_z(\rho_n)]^{\mathrm{T}}. \tag{81}$$

The matrices and the vector $\mathbf{A}^{(1)}$, $\mathbf{B}_-^{(1)}$, and $\mathbf{u}_1$ are specified according to the boundary condition at the origin, depending on the value of m. The singularity at the origin does not matter if the central difference is used, because Eqs. (4) and (5) are evaluated at the mid points between grids. The value of $\mathbf{u}$ at the origin is also given by Eqs. (15)–(17), which lead to

$$\mathbf{A}^{(1)} = \begin{bmatrix} \cdot & \cdot \\ -1 & \cdot \\ \cdot & \cdot \\ \cdot & -1 \end{bmatrix}, \quad \mathbf{B}_-^{(1)} = \begin{bmatrix} B_{1,2}^{(1)} & B_{1,4}^{(1)} \\ B_{2,2}^{(1)} & B_{2,4}^{(1)} \\ B_{3,2}^{(1)} & B_{3,4}^{(1)} \\ B_{4,2}^{(1)} & B_{4,4}^{(1)} \end{bmatrix}, \tag{82}$$

and

$$\mathbf{A}^{(1)} = \begin{bmatrix} -1 & \cdot \\ \cdot & \cdot \\ \cdot & -1 \\ \cdot & \cdot \end{bmatrix}, \quad \mathbf{B}_-^{(1)} = \begin{bmatrix} B_{1,1}^{(1)} & B_{1,3}^{(1)} \\ B_{2,1}^{(1)} & B_{2,3}^{(1)} \\ B_{3,1}^{(1)} & B_{3,3}^{(1)} \\ B_{4,1}^{(1)} & B_{4,3}^{(1)} \end{bmatrix}, \tag{83}$$

for $m = 0$ and $m = \pm 1$, respectively. The vector $\mathbf{u}_1$ is $[E_z(0), \mathcal{H}_z(0)]^{\mathrm{T}}$ for $m = 0$ or $[E_\theta(0), \mathcal{H}_\theta(0)]^{\mathrm{T}}$ for $m = \pm 1$. For $|m| > 1$, the system of equations is obtained by deleting the first two rows and two columns of the matrices $\mathbf{A}$ and $\mathbf{B}$

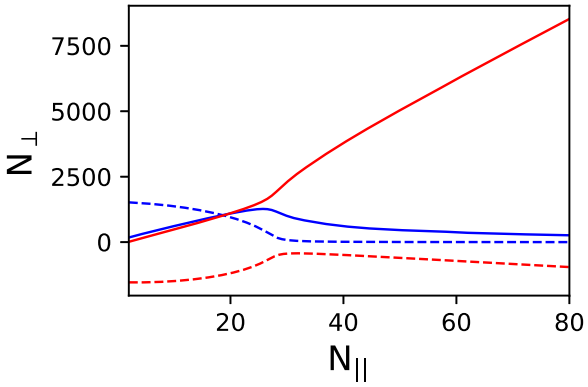

FIG. 1. The normalized perpendicular wave numbers given as functions of $N_\parallel$ for a uniform plasma. The real and imaginary parts are indicated by the solid and dashed lines, respectively.

and the first two rows of the vectors $\mathbf{U}$ and $\mathbf{R}$, as in the spectral method. The boundary conditions given by Eqs. (35) and (36) yield

$$\mathbf{A}^{(n-1)} = \begin{bmatrix} \mathbf{I}_2 \\ \mathbf{b} \end{bmatrix}, \tag{84}$$

$$\mathbf{B}_+^{(n-1)} = \hat{\mathbf{B}} + \tilde{\mathbf{B}} \cdot \mathbf{b}, \tag{85}$$

$$\mathbf{R} = [\cdots, -(\tilde{\mathbf{B}} + \mathbf{I}_2) \cdot \mathbf{d}]^{\mathrm{T}}, \tag{86}$$

where

$$\hat{\mathbf{B}} = \begin{bmatrix} B_{1,1}^{(n)} & B_{1,2}^{(n)} \\ B_{2,1}^{(n)} & B_{2,2}^{(n)} \\ B_{3,1}^{(n)} & B_{3,2}^{(n)} \\ B_{4,1}^{(n)} & B_{4,2}^{(n)} \end{bmatrix}, \quad \tilde{\mathbf{B}} = \begin{bmatrix} B_{1,3}^{(n)} & B_{1,4}^{(n)} \\ B_{2,3}^{(n)} & B_{2,4}^{(n)} \\ B_{3,3}^{(n)} & B_{3,4}^{(n)} \\ B_{4,3}^{(n)} & B_{4,4}^{(n)} \end{bmatrix}, \tag{87}$$

$$\mathbf{b} = \begin{bmatrix} b_{1,1} & b_{1,2} \\ b_{2,1} & b_{2,2} \end{bmatrix}, \quad \mathbf{d} = \begin{bmatrix} d_1 \\ d_2 \end{bmatrix}. \tag{88}$$

V. RESULTS

For illustrating the results, numerical calculations are conducted with the following parameters: plasma density

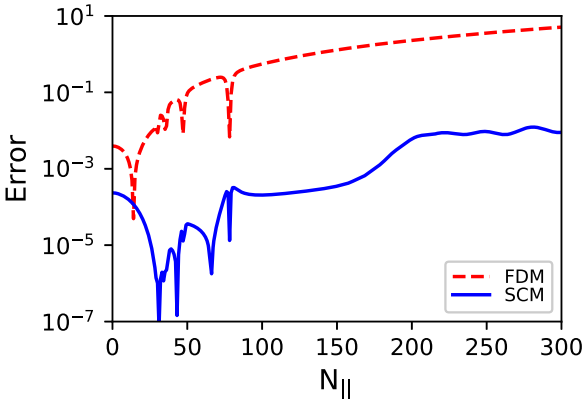

FIG. 2. Relative errors of the numerical solutions obtained by the finite difference and spectral collocation methods with respect to the analytic solution. These are denoted by FDM and SCM, respectively.

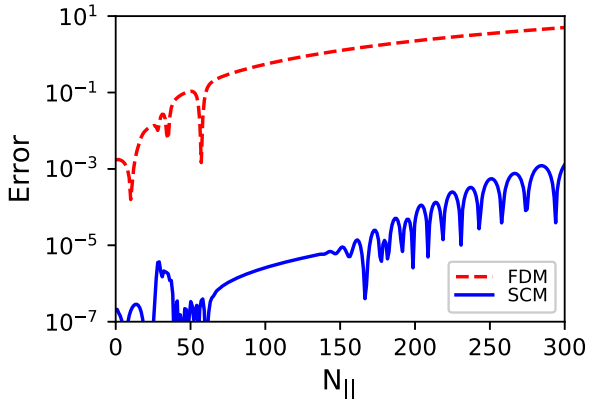

FIG. 3. Relative errors of power conservation for the numerical solutions obtained by the finite difference and spectral methods. The plasma is not uniform with $\mu = 2.2$, but other parameters are the same as in Fig. 2.

$n_0 = 5 \times 10^{12}$ cm^{-3}, magnetic field $B_0 = 500$ G, wave frequency $f = 13.56$ MHz, azimuthal mode number $m = 0$, electron-neutral collision frequency of $\nu/\omega = 0.1$, and plasma radius $r_p = 5$ cm, antenna radius $r_a = 6$ cm, conductor boundary radius $r_b = 10$ cm, and 100 subintervals, unless stated otherwise. Ion collisions are neglected. Numerical methods are compared for uniform and nonuniform plasmas with the density profile

$$n(r) = n_0 J_0\left(\mu \frac{r}{r_p}\right), \tag{89}$$

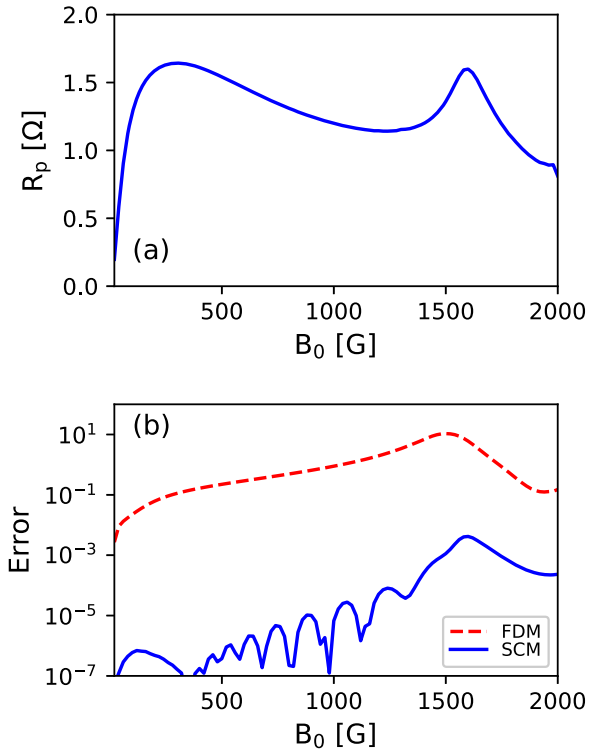

FIG. 4. (a) Plasma resistance from the spectral method and (b) the relative errors of power conservation from both methods given as functions of the magnetic field.

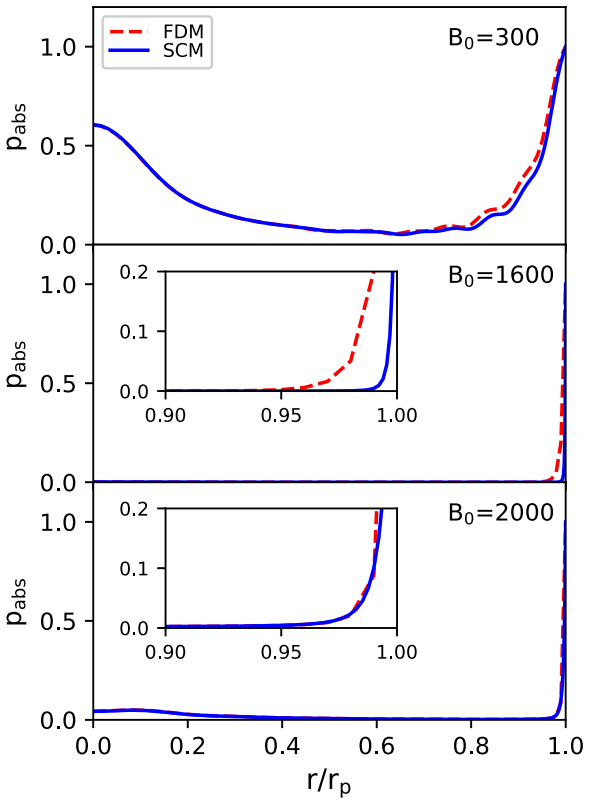

FIG. 5. Comparisons of the power absorption profiles between the finite difference and spectral methods at $B_0 = 300$, 1600, and 2000 G, respectively. The profiles are normalized to their respective maximum values.

where J_0 is the zeroth-order Bessel function.

Figure 1 presents $N_\perp$ as functions of $N_\parallel$ for a uniform plasma: $N_\perp$ of the TG mode becomes large as $N_\parallel$ increases, which may bring inaccuracy into numerical results at large values of $N_\parallel$. The accuracy of the numerical methods is examined by comparison with the analytic solutions for a uniform plasma. Relative errors are compared in Fig. 2, which shows that the finite difference method (FDM) does not give acceptable solutions except for the relatively very small values of $N_\parallel$ for given grid points, while the spectral method yields fairly accurate solutions over a wide range of $N_\parallel$.

For inhomogeneous plasmas, the accuracy of calculation can be checked by monitoring power conservation on how the values of S_a and S_p agree with each other. Figure 3 shows the relative difference $|1 - S_p/S_a|$. The FDM yields inaccurate solutions except for a very narrow range of $N_\parallel$, the same as for the uniform case, unless the number of grid points is increased.

Figure 4 shows the plasma resistance and the relative errors of power conservation as functions of the magnetic field for the density profile with $\mu = 2.2$. The accuracy of both methods decreases near the magnetic field, giving a peak resistance around 1600 G. This peak is related to the lower hybrid resonance [10].

If the magnetic field, the density, or the wave frequency is in the range of the resonance, there can be a resonance layer somewhere for a nonuniform density profile. When this layer

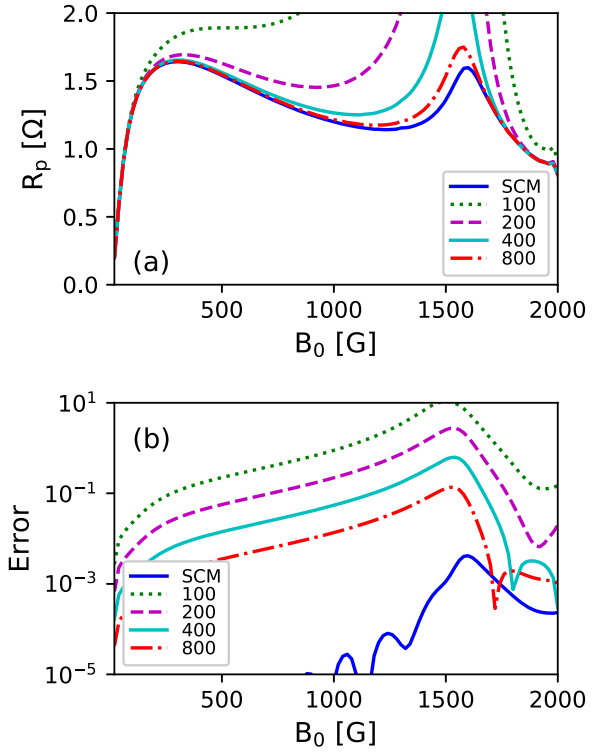

FIG. 6. Plasma resistance and its accuracy of the FDM compared with those of the spectral method. The numbers denote the number of subintervals used in the FDM. For the spectral method, the number of subintervals is 100.

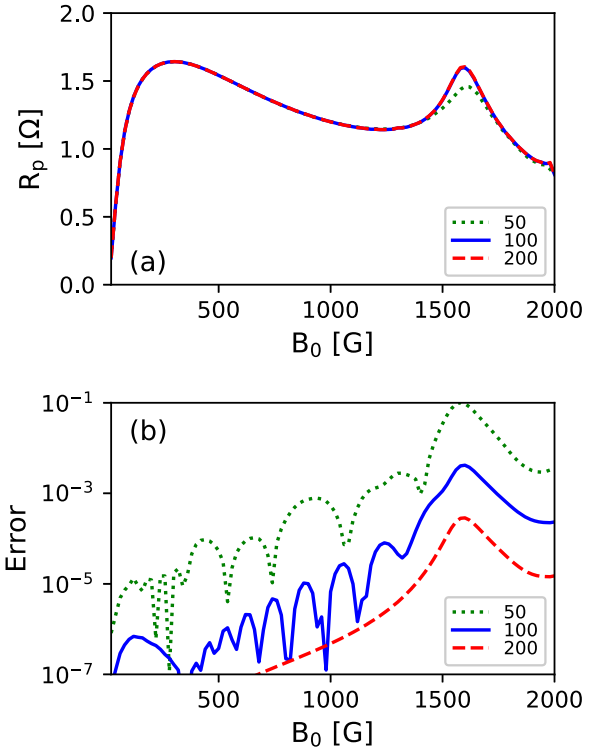

FIG. 7. Plasma resistance from the spectral method and its accuracy given as functions of the magnetic field for different numbers of subintervals.

is close to the boundary, the TG mode is damped strongly as it propagates inward and the power absorption is localized in the narrow region near the plasma boundary. The power absorption profile $p_{\rm abs}$ is compared at different magnetic fields in Fig. 5, where

$$P_{\rm abs} = \int_0^{r_p} p_{\rm abs} r\, dr, \tag{90}$$

$$p_{\rm abs} = 2\pi^2 \epsilon_0 \omega \int_{-\infty}^{\infty} {\rm Im}[\mathbf{E}^* \cdot \boldsymbol{\epsilon} \cdot \mathbf{E}]\, dk. \tag{91}$$

The value of $N_\perp$ of the TG mode increases as the magnetic field increases toward the lower hybrid resonance, and then it decreases when the magnetic field exceeds its value for the resonance [10]. Accordingly, the absorption profile shrinks to the narrower region near the boundary as the magnetic field increases up to the value giving the peak resistance, and then it becomes slightly wider as the magnetic field increases further. Errors are large around this value of the magnetic field, because the absorption profile is extremely localized near the edge.

The grid size should be small enough to resolve the wavelength to obtain better accuracy when the radial variation of the wave field is very large such as at high magnetic fields or near the resonance condition. Figure 6 shows that the results of the FDM converge to those of the spectral method as the number of grid points increases. The FDM does not yield accurate solutions near the resonance condition, unless the mesh size is very small there. The number of grid points is also varied to confirm that the spectral method converges faster with fewer grid points than in the FDM, as shown in Fig. 7.

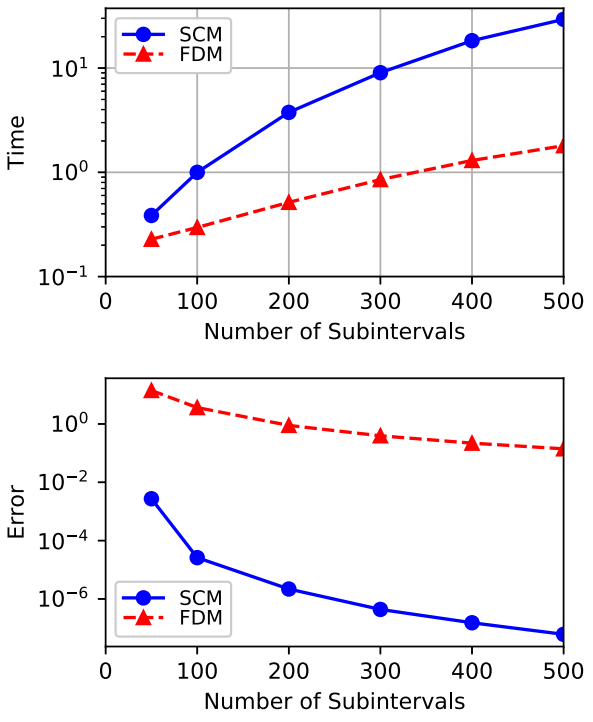

FIG. 8. Relative time and error versus the number of subintervals when $B_0 = 1000$ G and $N_\parallel = 100$. The time is normalized with respect to that of the spectral method with 100 subintervals.

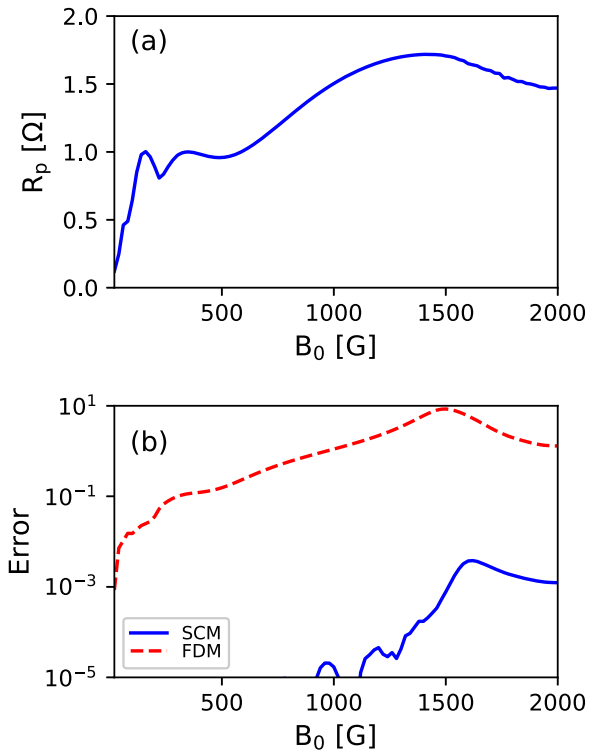

FIG. 9. Plasma resistance from the spectral method and relative errors of the spectral and the finite difference methods when the electromagnetic fields are excited by a Nagoya Type III antenna. The $m = \pm 1$ modes are included, and the other parameters are the same as in Fig. 4.

Because the net power transfer to the plasma is proportional to $R_p/(R_p + R_c)$, where R_c is the resistance resulting from conduction loss [46], discharge at high R_p is usually desired in practice for high ionization efficiency. The plasma resistance is large in general when the TG mode damps within a narrow layer near the edge, yielding surface heating [47]. Therefore, the spectral collocation method is especially advantageous when the FDM gives inaccurate results, such as in the case where the plasma resistance is relatively large.

The spectral method generates the full matrices, resulting in longer computing times than the FDM, where sparse linear equations are solved for the same number of nodes. Computing times and errors are compared in Fig. 8 for the finite difference and spectral methods for different numbers of subintervals when $B_0 = 1000$ G and $N_\parallel = 100$. The time is normalized with respect to that of the spectral method with 100 subintervals, which takes slightly less time than the finite difference method with 400 subintervals, yielding very accurate results. The dependence of time and error on the number of subintervals is quite general, irrespective of the parameter values. In spite of the full matrices, the Chebyshev spectral collocation method seems to be best suited for analysis of the electromagnetic waves in helicon plasmas, because it has excellent accuracy with rapid convergence with the node number and, more importantly, highly clustered nodes near the plasma boundary as well.

The superiority of the spectral method is not limited to a particular azimuthal mode. Figure 9 shows the resistance and the relative errors for the case of a Nagoya Type III antenna, which excites primarily $m = \pm 1$ modes [34].

VI. CONCLUSIONS

The spectral collocation method with the Chebyshev differentiation matrix is applied to compute the electromagnetic fields and the collisional power absorption in radially inhomogeneous helicon plasmas. The governing equation has a singularity at the origin, which has been resolved by imposing the boundary condition that the field components should be independent of the azimuthal angle there. The accuracy of the Chebyshev spectral collocation method is outstanding in comparison with the finite difference method. It appears to be best suited to analysis of electromagnetic waves in helicon plasmas, because it has excellent accuracy with rapid convergence with the number of nodes and, more importantly, highly clustered nodes near the plasma boundary, where the TG mode varies rapidly with significant damping when the power absorption is strong. It is possible to extend the range of parameters such as magnetic field, plasma density, and frequency, for which the FDM fails to obtain reliable solutions without drastically decreasing the grid size. The spectral collocation method is especially useful when the parameters are in the range of the lower hybrid resonance

ACKNOWLEDGMENT

This work was supported by Kyonggi University Research Grant 2017.

[1] R. W. Boswell, Plasmas Phys. Control. Fusion **26**, 1147 (1984).
[2] J.-G. Kwak, H. D. Choi, H. I. Bak, S. Cho, J. S. Bak, and S. K. Kim, Phys. Plasmas **4**, 1463 (1997).
[3] K.-K. Chi, T. E. Sherican, and R. W. Boswell, Plasma Sources Sci. Technol. **8**, 421 (1999).
[4] F. F. Chen, X. Jiang, J. D. Evans, G. Tynan, and D. Arnush, Plasmas Phys. Control. Fusion **39**, A411 (1997).
[5] F. F. Chen, Phys. Plasmas **10**, 2586 (2003).
[6] T. Lafleur, C. Charles, and R. W. Boswell, Phys. Plasmas **17**, 043505 (2000).
[7] S. Cho, Phys. Plasmas **13**, 033504 (2006).
[8] S.-M. Yun, J.-H. Kim, and H.-Y. Chang, J. Vac. Sci. Technol. A **15**, 673 (1997).
[9] Y. Sakawa, T. Takino, and T. Shoji, Phys. Plasmas **6**, 4759 (1999).
[10] S. Cho, Phys. Plasmas **7**, 417 (2000).
[11] J. G. Kwak, S. K. Kim, and S. Cho, Phys. Lett. A **267**, 384 (2000).
[12] S. Yun, S. Cho, G. Tynan, and H. Chang, Phys. Plasmas **8**, 358 (2001).
[13] S. Cho, Phys. Lett. A **216**, 137 (1996).
[14] K. P. Shamrai, Plasma Sources Sci. Technol. **7**, 499 (1998).

[15] F. F. Chen and H. Torreblanca, Plasma Sources Sci. Technol. **16**, 593 (2007).
[16] K. P. Shamrai and V. B. Taranov, Plasmas Phys. Control. Fusion **36**, 1719 (1994).
[17] K. P. Shamrai and V. B. Taranov, Plasma Sources Sci. Technol. **5**, 474 (1996).
[18] S. Cho, Phys. Plasmas **3**, 4268 (1996).
[19] Y. Mouzouris and J. E. Scharer, IEEE Trans. Plasma Sci. **24**, 152 (1996).
[20] S. Cho and J.-G. Kwak, Phys. Plasmas **4**, 4167 (1997).
[21] D. Arnush and F. F. Chen, Phys. Plasmas **5**, 1239 (1998).
[22] M. Krämer, Phys. Plasmas **6**, 1052 (1999).
[23] S. Shinohara and K. P. Shamrai, Plasmas Phys. Control. Fusion **42**, 865 (1994).
[24] D. Arnush, Phys. Plasmas **7**, 3042 (2000).
[25] K. P. Shamrai and S. Shinohara, Phys. Plasmas **8**, 4659 (2001).
[26] K. Niemi and M. Krämer, Phys. Plasma **15**, 073503 (2008).
[27] B. Soltani, M. Habibi, and H. Zakeri-khatir, Phys. Plasmas **23**, 023507 (2016).
[28] M. Kabir and A. Niknam, Phys. Plasmas **24**, 053511 (2017).
[29] M. Afsharmanesh and M. Habibi, IEEE Trans. Plasma Sci. **45**, 2272 (2017).
[30] I. V. Kamenski and G. G. Borg, Comput. Phys. Commun. **113**, 10 (1998).
[31] T. Enk and M. Krämer, Phys. Plasma **7**, 4308 (2000).
[32] B. H. Park, N. S. Yoon, and D.-I. Choi, IEEE Trans. Plasma Sci. **29**, 502 (2001).
[33] D. D. Blackwell, T. G. Madziwa, D. Arnush, and F. F. Chen, Phys. Rev. Lett. **88**, 145002 (2002).
[34] F. F. Chen, Plasma Sources Sci. Technol. **24**, 014001 (2015).
[35] Y. Mouzouris and J. E. Scharer, Phys. Plasmas **5**, 4253 (1998).
[36] G. Chen, A. V. Arefiev, R. D. Bengtson, B. N. Breizman, C. Lee, and L. L. Raja, Phys. Plasma **13**, 123507 (2006).
[37] S. Cho, Jour. Kor. Phys. Soc. **58**, 461 (2011).
[38] L. Chang, M. J. Hole, J. F. Caneses, G. Chen, B. D. Blackwell, and C. S. Corr, Phys. Plasma **19**, 083511 (2012).
[39] S. Cho, Phys. Plasmas **16**, 063504 (2009).
[40] B. McVey, *PFC/RR-84-12* (Plasma Fusion Center, MIT, Cambridge, MA, 1984).
[41] J. P. Boyd, *Chebyshev and Fourier Spectral Methods* (Dover, Mineola, NY, 2001).
[42] L. N. Trefethen, *Spectral Methods in Matlab* (SIAM, Philadelphia, 2000).
[43] J. A. C. Weideman and S. C. Reddy, ACM Trans. Math. Software **26**, 465 (2000).
[44] J. P. Boyd and F. Yu, J. Comput. Phys. **230**, 1408 (2011).
[45] M. Brambilla, Plasma Phys. Control. Fusion **41**, 1 (1999).
[46] T. Shoji, Y. Sakawa, S. Nakazawa, and T. Sato, Plasma Sources Sci. Technol. **2**, 5 (1993).
[47] S. Cho and M. A. Lieberman, Phys. Plasmas **10**, 882 (2003).